Zebrafish model for human long QT syndrome

Rima Arnaout[†‡], Tania Ferrer[§], Jan Huisken[†], Kenneth Spitzer[§], Didier Y. R. Stainier[†¶], Martin Tristani-Firouzi[§¶], and Neil C. Chi[†¶]

[†]Department of Biochemistry and Biophysics, Programs in Developmental Biology, Genetics, and Human Genetics, Cardiovascular Research Institute, University of California, 1550 Fourth Street, San Francisco, CA 94158; [§]Department of Pediatrics and Nora Eccles Harrison Cardiovascular Research and Training Institute, University of Utah, 95 South 2000 East, Salt Lake City, UT 84112; and [‡]Harvard Medical School, 260 Longwood Avenue, Boston, MA 02115

Edited by David E. Clapham, Harvard Medical School, Boston, MA, and approved May 21, 2007 (received for review March 23, 2007)

Long QT syndrome (LQTS) is a disorder of ventricular repolarization that predisposes affected individuals to lethal cardiac arrhythmias. To date, an appropriate animal model of inherited LQTS does not exist. The zebrafish is a powerful vertebrate model used to dissect molecular pathways of cardiovascular development and disease. Because fundamental electrical properties of the zebrafish heart are remarkably similar to those of the human heart, the zebrafish may be an appropriate model for studying human inherited arrhythmias. Here we describe the molecular, cellular, and electrophysiological basis of a zebrafish mutant characterized by ventricular asystole. Genetic mapping and direct sequencing identify the affected gene as *kcnh2*, which encodes the channel responsible for the rapidly activating delayed rectifier K^+ current (I_{Kr}). We show that complete loss of functional I_{Kr} in embryonic hearts leads to ventricular cell membrane depolarization, inability to generate action potentials (APs), and disrupted calcium release. A small hyperpolarizing current restores spontaneous APs, implying wild-type function of other ionic currents critical for AP generation. Heterozygous fish manifest overt cellular and electrocardiographic evidence for delayed ventricular repolarization. Our findings provide insight into the pathogenesis of homozygous *kcnh2* mutations and expand the use of zebrafish mutants as a model system to study human arrhythmias.

cardiac | development | kcnh2 | arrhythmia | electrophysiology

Autosomal dominant *KCNH2* mutations account for ≈45% of mutation-positive long QT syndrome (LQTS) (1, 2). Recessive *KCNH2* mutations are rarely reported, implying that most homozygous mutations are embryonic-lethal (3, 4). The cellular mechanisms underlying embryonic lethality are not known. Although LQTS has been extensively characterized in humans, establishing an animal model would be helpful to identify genes that modify phenotypic expressivity or to screen against compounds that cause acquired forms of LQTS. To date, an appropriate animal model of inherited LQTS does not exist. Transgenic strategies and targeted deletion of genes that regulate rapidly activating delayed rectifier K^+ current (I_{Kr}) and slow delayed rectifier K^+ current (I_{Ks}) in mice fail to produce a significant phenotype (5–7). The mouse heart rate is nearly 10 times faster than that of humans, and thus a distinct cadre of ion channels facilitates ventricular repolarization in mice (5–8).

Although the zebrafish heart is two-chambered, its fundamental electrical properties are remarkably similar to those of humans (9). For example, embryonic and adult heart rates are similar to those of humans (10, 11), and the relationship between QT interval and heart rate parallels that of humans (11). Forward-genetic screens using zebrafish have identified many cardiovascular mutants for analysis (12, 13), thereby revealing critical pathways in cardiovascular development that parallel those of higher vertebrates (14). Large clutch size facilitates positional cloning and other high-throughput experiments using zebrafish embryos and larvae. The role of zebrafish mutants as models of human-inherited arrhythmia has not yet been established.

In this study, we analyze the molecular, cellular, and electrophysiological bases of two recessive mutations that cause ventricular asystole (silent ventricle). The silent ventricle phenotype is characterized by disrupted intracellular calcium release and can be rescued with an injection of hyperpolarizing current. Like their human counterparts, heterozygous animals exhibit increased sensitivity to QT-prolonging drugs, ventricular action potential (AP) prolongation, and QT interval prolongation on an electrocardiogram.

Results and Discussion

Mutations in *kcnh2* Cause a Silent Ventricle Phenotype and Render I_{Kr} Channels Nonfunctional. We identified two alleles (*s213* and *s290*) of a silent ventricle mutant in an ethylnitrosourea forward-genetic screen (15). As early as 33 h postfertilization (hpf), the mutant ventricles do not contract or fill with blood, appearing collapsed. Atrial contraction and morphology appear unaffected. By 48 hpf, both mutant alleles also exhibit pericardial edema and absence of circulation [Fig. 1 *b* and *c* and supporting information (SI) Movies 1 and 2]. After several days, the atrium contracts only weakly, and pericardial edema has increased, ultimately resulting in death by ≈10 days postfertilization, when the larva can no longer survive on oxygen diffusion alone. By contrast, heterozygotes survive to adulthood and are fertile.

We genetically mapped the *s290* mutation to a 1.8-cM region on chromosome 3 and identified a zero-recombinant marker within *kcnh2* (Fig. 1*d*). Sequence analysis of *kcnh2* revealed missense mutations in the *s213* and *s290* mutant alleles, resulting in Ile462Arg and Met521Lys substitutions in the S3 and S5 transmembrane domains, respectively (Fig. 1 *e* and *f*). To further test whether *kcnh2* was responsible for the silent ventricle phenotype of the *s213* and *s290* mutants, we knocked down its function by using morpholino antisense oligonucleotides. Injection of 2 ng of an ATG morpholino recapitulated the silent ventricle phenotype in ≈95% of embryos ($n > 150$). Moreover, injecting 100 pg of wild-type *kcnh2* mRNA into *s290* embryos rescued the silent ventricle phenotype in 83% of homozygous mutant embryos ($n = 47$; SI Fig. 6). Through complementation analysis, we determined that *s213* and *s290* are strong alleles of bre^{tb218}, which was identified as a mutation in *kcnh2* (16). Together these data indicate that the *s213* and *s290* mutations affect *kcnh2*.

To determine the functional consequences of the disease-causing mutations, we recorded ionic currents from wild-type and mutant Kcnh2 heterologously expressed in *Xenopus* oocytes. Wild-type zebrafish Kcnh2 current displayed biophysical fea-

Author contributions: R.A., T.F., J.H., D.Y.R.S., M.T.-F., and N.C.C. designed research; R.A., T.F., J.H., K.S., M.T.-F., and N.C.C. performed research; R.A., T.F., J.H., D.Y.R.S., M.T.-F., and N.C.C. analyzed data; and R.A., D.Y.R.S., M.T.-F., and N.C.C. wrote the paper.

The authors declare no conflict of interest.

This article is a PNAS Direct Submission.

Abbreviations: hpf, hours postfertilization; LQTS, long QT syndrome; LQT2, LQTS type 2; AP, action potential; I_{Kr}, rapidly activating delayed rectifier K^+ current; I_{Ks}, slow delayed rectifiers K^+ current; SPIM, selective plane illumination microscopy.

[¶]To whom correspondence may be addressed. E-mail: didier_stainier@biochem.ucsf.edu, mfirouzi@cvrti.utah.edu, or chi@medicine.ucsf.edu.

This article contains supporting information online at www.pnas.org/cgi/content/full/0702724104/DC1.

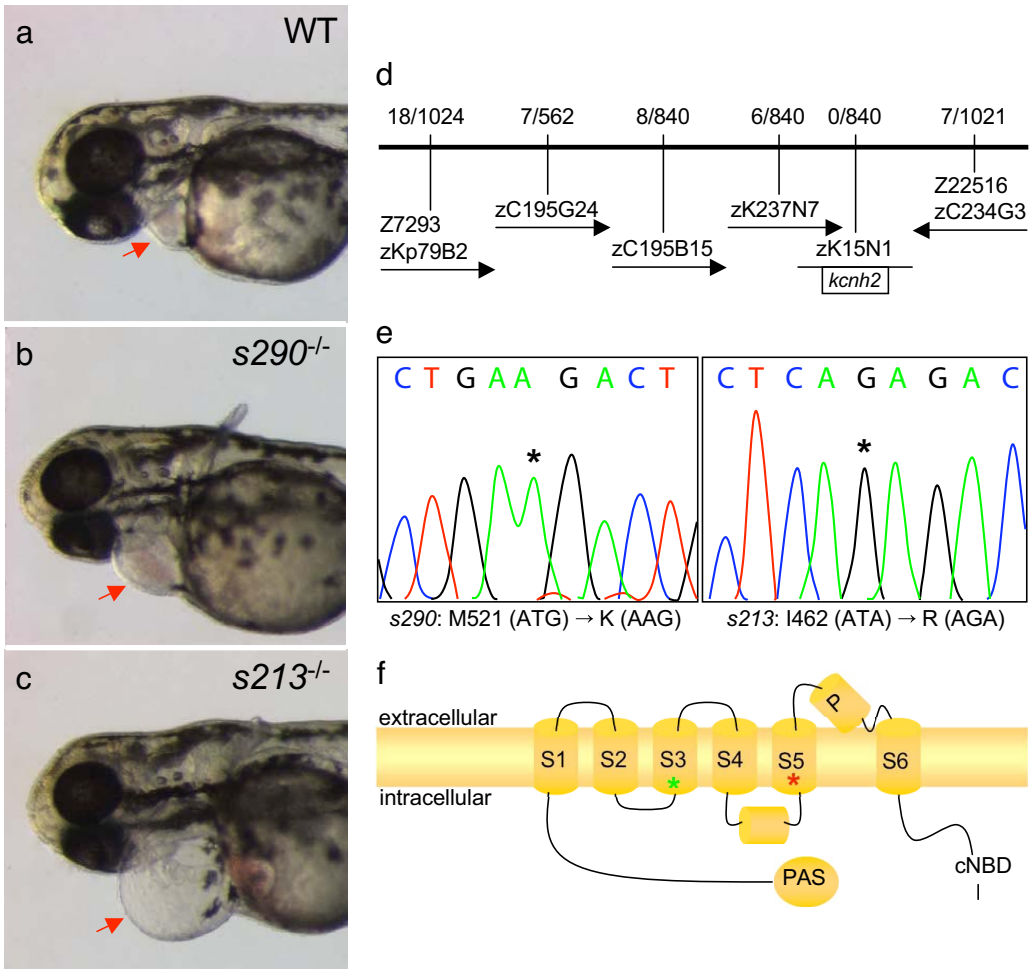

Fig. 1. Molecular analysis of two *kcnh2* mutant alleles. (*a–c*) Wild-type and mutant embryos at 48 hpf, lateral oblique views, anterior to the left. Compared with wild type (WT) (*a*), *s213* (*b*), and *s290* (*c*), mutants exhibit a silent ventricle and, therefore, absent cardiac output and pronounced pericardial edema (red arrows). (*d*) The mutations map to linkage group 3. Flanking CA repeat markers and markers from selected BACs are shown, with the number of recombinants for the given number of meioses. The *s213* and *s290* mutations map to the potassium channel gene *kcnh2*. (e) Sequence analysis of *kcnh2* in *s213* mutants reveals a T–G transition at codon 462, resulting in an Ile–Arg substitution. For *s290*, a T–A transversion at codon 521 results in a Met–Lys substitution. (*f*) Schematic diagram showing the modular structure of Kcnh2. A Kcnh2 subunit consists of six transmembrane domains: the S1–S4 domains sense membrane potential, whereas the S5–S6 domains form the K-selective pore. Green and red stars represent the *s213* and *s290* mutation sites, respectively.

tures similar to those of human KCNH2 (17), including slowly activating, rapidly inactivating current (Fig. 2). Ile462Arg and Met521Lys Kcnh2 induced currents similar in magnitude to those observed in water-injected oocytes, consistent with complete loss of channel function (Fig. 2). Thus, the functional analyses of these mutations predict a complete loss of I_{Kr} function in the homozygous mutant embryos.

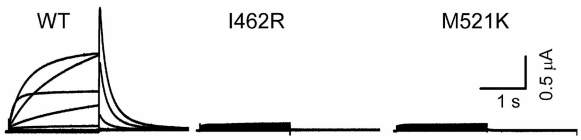

Fig. 2. *kcnh2* mutations cause complete loss of channel function. Representative ionic currents recorded from wild-type (WT), I462R, and M521K Kcnh2 heterologously expressed in *Xenopus* oocytes. Currents were elicited by 2-sec voltage steps between −80 and +40 mV applied from a holding potential of −80 mV. Deactivating tail currents were elicited by a 2-sec voltage step to −70 mV. Currents induced by I462R and M521K mutant Kcnh2 were no different from those seen in water-injected oocytes, indicating complete loss of channel function.

Homozygous *kcnh2* Mutant Embryonic Ventricle Does Not Generate Spontaneous APs. To determine how the complete loss of functional I_{Kr} results in ventricular asystole, we recorded APs from wild-type and mutant explanted embryonic hearts by using patch pipettes and a current clamp technique. The morphology of APs recorded from a wild-type atrium was similar to that reported for mammalian sino-atrial node, with phase 4 depolarization triggering spontaneous APs (Fig. 3*a* and SI Table 1). Wild-type ventricular APs displayed a more negative diastolic transmembrane voltage (V_m) and longer duration than atrial APs (SI Table 1). The ventricular AP duration was calculated as the time interval between the peak maximum upstroke velocity (phase 0) and the time at 90% of repolarization (APD_{90}). The ventricular APD_{90} was 272 ± 15 msec (n = 14), similar to the duration of monophasic APs recorded from human ventricle (250–260 msec) (18). The relatively slow maximal upstroke velocity (SI Table 1) and the upstroke inhibition by nifedipine, but not tetrodotoxin (data not shown), imply that AP upstroke in both the atrium and ventricle is largely dependent on L-type Ca^{2+} currents. These findings are consistent with the L-type Ca^{2+}-dependent APs reported from early differentiated mammalian cardiomyocytes (19).

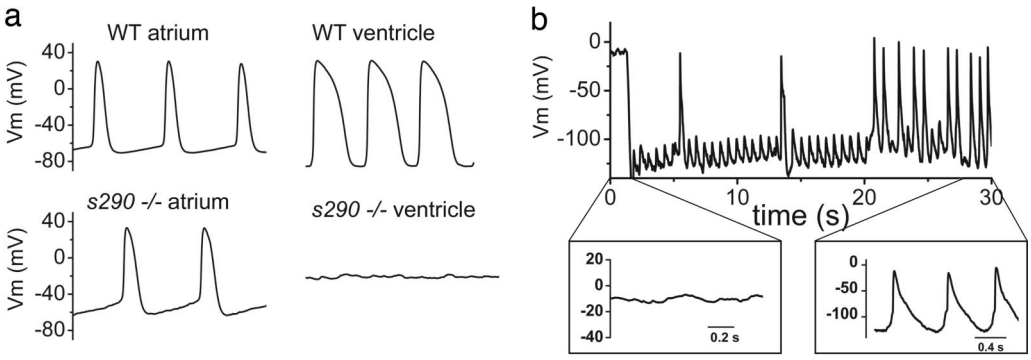

Fig. 3. APs recorded from explanted embryonic zebrafish hearts. (*a*) (*Upper*) Representative spontaneous APs recorded from wild-type (WT) atrium (*Left*) and ventricle (*Right*) at 48 hpf. (*Lower*) Spontaneous APs recorded from *kcnh2*^{s290} mutant atrium (*Left*). Recordings of transmembrane voltage (V_m) from mutant ventricle (*Right*) revealed marked membrane depolarization and the absence of action potentials. (*b*) V_m recorded from *kcnh2*^{s290} mutant ventricle. Intracellular injection of hyperpolarizing current (−100 pA) caused membrane hyperpolarization and allowed for the generation of spontaneous APs.

Mutant atria also generated spontaneous APs, although the cycle length, AP duration, and effective refractory period were longer than wild type (SI Table 1). This observation implies that I_{Kr} participates in setting the pacemaker rate and contributes to phase 3 repolarization in the atrium. Recordings from mutant ventricles were markedly abnormal, with a resting V_m of −0.5 ± 3 mV (n = 10), compared with −70 mV in wild type (SI Table 1). No spontaneous APs were detected in mutant ventricles, even as the atria were contracting vigorously. This degree of cell membrane depolarization would be expected to inactivate ventricular Ca^{2+} channels responsible for AP upstroke. To determine whether the mutant ventricle was functionally capable of generating APs, we restored the membrane potential with continuous injection of a small negative current (50–100 pA). This current caused hyperpolarization of V_m to less than −80 mV, at which point spontaneous APs were consistently elicited (Fig. 3*b*). The resultant APs were markedly abnormal, with the repolarization phase (see Fig. 3*b Inset*) provided not by K^+ current, but rather by the injected, hyperpolarizing current. These data suggest that the mutant ventricle is functionally capable of generating APs, but that the complete absence of I_{Kr} causes membrane depolarization, which inactivates L-type Ca^{2+} channels and inhibits AP upstroke.

To further explore the role of I_{Kr} in modulating ventricular APs, we perfused explanted embryonic hearts with high (1 μM) and low (100 nM) terfenadine concentrations, expecting to cause maximal and submaximal I_{Kr} block, respectively (20). High concentrations of terfenadine (1 μM) caused progressive depolarization of ventricular V_m (−75 ± 9 to −52 ± 6 mV; n = 3) and diminished AP magnitude, and subsequently eliminated electrical activity, similar to the *s213* and *s290 kcnh2* mutations (SI Fig. 7). Lower concentrations of terfenadine (100 nM) prolonged AP duration by 58 ± 15% (n = 4), resulting in a 2:1 block of external pacing (SI Fig. 7). Thus, a partial I_{Kr} block prolongs AP duration and reduces excitability, whereas a complete I_{Kr} block eliminates excitability in an embryonic zebrafish ventricle. Moreover, these data imply that I_{Kr} is not only critical for repolarization, but is also important for maintaining resting V_m in the embryonic ventricle.

***kcnh2* Homozygous Mutant Ventricle Has Impaired Ca^{2+} Release.** The effect of the null *kcnh2* mutations on cardiac Ca^{2+} cycling was studied in the zebrafish transgenic line *Tg(cmlc2:gCaMP)*^{s878} (N.C.C., R. M. Shaw, B. Jungblut, J.H., R.A., T.F., M.T.-F., L. J. Jan, and D.Y.R.S., unpublished data), which expresses gCaMP, a genetically encoded, voltage-sensitive fluorescent Ca^{2+} sensor (21), using selective plane illumination microscopy (SPIM) (22) to image fluctuating Ca^{2+} in the heart with high spatial and temporal resolution. To facilitate imaging, contraction was uncoupled from conduction by injection of the silent heart cardiac troponin (*tnnt2*) morpholino (23) at the one-cell stage. *In vivo* images were then obtained at 48 hpf. In wild-type *tnnt2* morpholino-injected *Tg(cmlc2:gCaMP)*^{s878} hearts, repetitive fluorescent waves representing systolic Ca^{2+} release were visible spreading from the atrium through the atrioventricular junction and into the ventricle (Fig. 4a and SI Movie 3). In *tnnt2* morpholino-injected *Tg(cmlc2:gCaMP)*^{s878} *kcnh2*^{s213} and -*kcnh2*^{s290} homozygous mutant embryos, Ca^{2+} waves were visible in the atrium, but no fluorescent changes were detected in the ventricle (Fig. 4*b* and SI Movie 4). These data indicate that Ca^{2+} release and/or reuptake is impaired in *kcnh2* mutant ventricular myocytes as a consequence of absent I_{Kr}.

***kcnh2* Heterozygous Animals Display Abnormal Ventricular Repolarization.** Heterozygous *kcnh2*^{s213} and *kcnh2*^{s290} embryos appear phenotypically similar to their wild-type siblings. However, when coexpressed with wild-type *kcnh2* at equimolar mRNA concentrations, Ile462Arg and Met521Lys *kcnh2* caused reduced current consistent with dominant-negative suppression of wild-type Kcnh2 channel function (data not shown), suggesting that I_{Kr} function may be reduced in the heterozygous state. To determine whether heterozygous fish, like their human LQT2 counterparts, are especially sensitive to I_{Kr}-blocking drugs, we bathed 48 hpf embryos with terfenadine (24). At increasing concentrations, terfenadine causes bradycardia, a 2:1 atrioventricular block, and ultimately ventricular asystole in embryonic zebrafish hearts (11, 16, 25). For these experiments, high concentrations of terfenadine were required to observe an effect given that the compound must diffuse through the embryo. We chose a terfenadine concentration (32 μM) that was below the threshold (85 μM, 2-h incubation) for development of a 2:1 block in wild-type embryonic hearts. Wild-type-looking embryos from incrossed *kcnh2*^{s213} and *kcnh2*^{s290} heterozygous fish were incubated in 32 μM terfenadine, scored for the development of a 2:1 block, and genotyped. For each allele, 100% (n = 12) of the heterozygotes developed a 2:1 heart block, as opposed to none of the homozygous wild-type embryos (n = 9). In this setting, heart block presumably occurs as a consequence of refractory ventricular myocardium, rather than a block at the level of the atrioventricular node/groove. Likewise, children with severe LQTS often present in the newborn period with a functional 2:1 atrioventricular heart block because of markedly delayed ventricular repolarization (3).

Our data suggest that *kcnh2*^{s213} and *kcnh2*^{s290} heterozygous embryos have reduced repolarization reserve. To determine whether heterozygotes are distinguishable from wild type at the

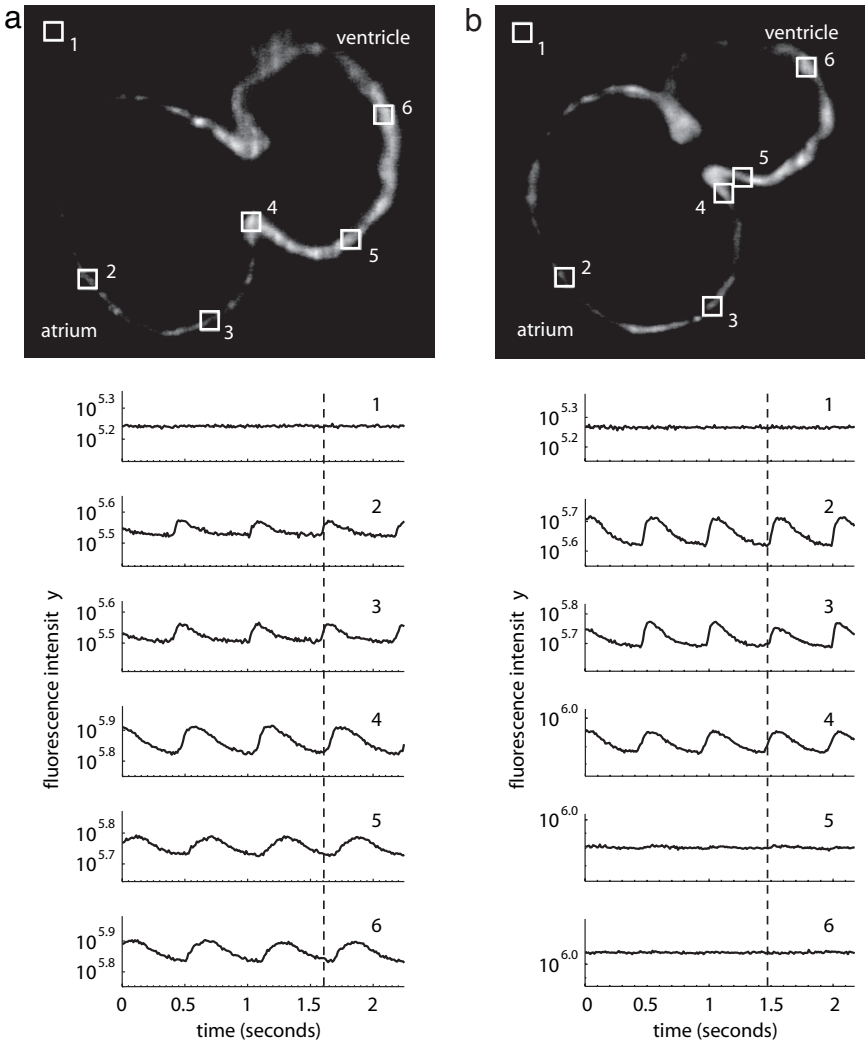

Fig. 4. Wild-type embryonic hearts in the *Tg(cmlc2:gCaMP)*^{s878} background exhibit atrial and ventricular conduction waves, whereas mutant hearts exhibit atrial, but no ventricular, conduction waves. SPIM videos of live 48 hpf hearts in the *Tg(cmlc2:gCaMP)*^{s878} background (see SI Movies 3 and 4) were processed to determine the fluorescence intensity of selected regions of the heart over time. Each selected region has a corresponding number plotted below. The dotted lines mark an arbitrary point in time to facilitate comparison across the different plots. (*a*) In a wild-type heart, fluorescence intensity varies with time in atrial and ventricular regions of the heart as the wave of depolarization propagates through the heart. This wave represents a wild-type heart rhythm. (*b*) In a *kcnh2*^{s290} mutant heart, fluorescence intensity varies in the atrium, but the ventricle maintains a constant, low-level intensity. The mutant heart lacks a ventricular conduction wave.

cellular level, we recorded APs from wild-type and *kcnh2*^{s290} heterozygous embryonic ventricles. Embryos were genotyped after APD_{90} was determined in a blinded fashion. APD_{90} measured from *kcnh2*^{s290} heterozygous ventricles (476 ± 35 msec; $n = 4$) was longer than wild type (330 ± 12 msec; $n = 8$; $P < 0.001$; Fig. 5*a*). These data confirm that repolarization reserve is reduced in heterozygous embryos and explain why heterozygotes are more sensitive to terfenadine compared with their wild-type siblings.

Finally, to determine whether adult heterozygous zebrafish are phenotypically distinguishable from wild-type fish, we performed electrocardiograms (Fig. 5*b*) using a protocol similar to that reported by Milan *et al*. (11). The QT interval is a measure of the duration of ventricular repolarization and is defined as the time from the upstroke of the QRS complex (the onset of depolarization) to the end of the T wave (termination of repolarization). To determine the relationship between QT interval and heart rate, the QT and RR intervals were plotted and fitted to the equation $QT = QTc*RR^{\alpha}$ to determine an α-value of 0.58 ($n = 18$; $R^2 = 0.89$). The QT interval was corrected for heart rate by using the equation $QTc = QT/RR^{\alpha}$. The mean QTc in adult wild-type zebrafish was 416 ± 8 msec ($n = 18$), which is remarkably similar to the normal value for humans (normal range 300–450 msec), further underscoring the electrical similarities between zebrafish and human hearts. Moreover, QTc measured from *kcnh2*^{s290} heterozygous fish (469 ± 25 msec; $n = 7$) was significantly longer than wild type ($P = 0.02$). Thus, adult *s290* heterozygous fish have delayed ventricular repolarization as manifested by prolongation of the QTc interval on the electrocardiogram.

Taken together, the data presented here offer a quantitative analysis of the consequences of *kcnh2* loss of function at an early developmental stage with a level of detail previously unobtainable in humans or mammalian model systems. Our study provides a potential mechanistic explanation as to why homozygous mutations in *KCNH2* are more rare than expected. Although the frequency of autosomal dominant mutations in *KCNH2* and *KCNQ1* (the gene encoding the channel responsible for the I_{Ks})

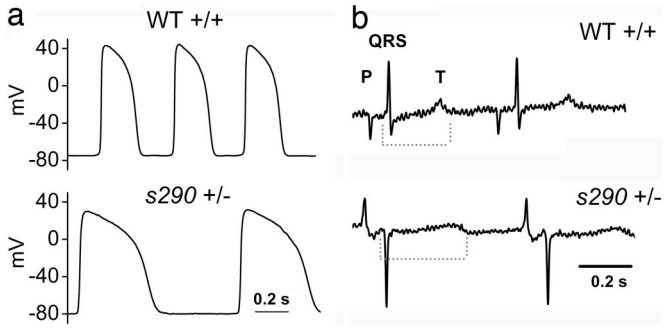

Fig. 5. Heterozygous *kcnh2* zebrafish manifest delayed ventricular repolarization. (*a*) APs recorded from 48 hpf heterozygous ventricle show increased AP duration compared with wild-type (see *Results*). (*b*) Representative electrocardiograms recorded from anesthetized, paralyzed wild-type and heterozygous adult zebrafish. Dashed line indicates duration of QT interval. QT corrected for heart rate (see *Materials and Methods*) was 396 and 467 msec for the exemplar wild-type and heterozygote, respectively.

is nearly equal, the frequency of homozygous mutations is disparate. The incidence of homozygous mutations in *KCNQ1* (also known as Jervell–Lange–Nielsen syndrome) is ≈1:500,000, with affected individuals manifesting severe QT prolongation and sensorineural deafness (26). By contrast, viable humans with homozygous *KCNH2* mutations are only rarely described in the literature, most likely as a consequence of embryonic lethality. Lethality in zebrafish *kcnh2* mutants occurs as the result of chronic membrane depolarization, with the resultant inability to generate APs and appropriately cycle intracellular Ca^{2+}. The precise cellular mechanisms underlying embryonic lethality in human homozygous LQT2 remain to be determined.

Heterozygous mutations in zebrafish *kcnh2* recapitulate the human LQTS phenotype as manifested by AP prolongation and prolonged QT interval, and thereby define the first animal genetic model of human LQT2. A major unanswered question within the LQTS field is why one affected individual manifests marked QT prolongation, whereas their sibling harboring the identical mutation appears phenotypically unaffected. As a model of LQT2, the zebrafish mutants described here offer the opportunity to analyze a large number of offspring with an identical *knch2* mutation and to ultimately identify comodifying genes that influence phenotypic expressivity in humans.

Materials and Methods

Zebrafish Strains and Lines. Zebrafish were raised under standard laboratory conditions at 28°C. We used the following lines: *kcnh2*^{s213} (15), *kcnh2*^{s290} (15), *tnnt2*^{b109} (23), *Tg(cmlc2:gCaMP)*^{s878} (N.C.C., R. M. Shaw, B. Jungblut, J.H., R.A., T.F., M.T.-F., L. J. Jan, and D.Y.R.S., unpublished data), and *Tg(cmlc2:eGFP)* (27).

Pharmacological Treatment. A 30-mM stock of terfenadine (Sigma–Aldrich, St. Louis, MO) in DMSO was diluted in embryo water. Embryos at 48 hpf were dechorionated, if not already hatched, and incubated in 1 to 85 μM terfenadine in embryo water. Control embryos were incubated in 1% DMSO in embryo water.

Mapping. We mapped the mutation to linkage group 3 by using a set of simple sequence-length polymorphism markers. For fine mapping, 840 mutant embryos were tested with simple sequence-length polymorphism markers in the critical region (Fig. 1*d*). *kcnh2* complementary DNA was isolated, sequenced, and analyzed from wild-type and the two mutant alleles. To genotype mutant embryos, we used a BsmA1 restriction site for restriction fragment length polymorphism analysis of *kcnh2*^{s213} and an Sml1 restriction site for restriction fragment length polymorphism analysis of *kcnh2*^{s290}.

Video Recording/Microscopy. Brightfield pictures and videos were taken by using a Stemi SV11 dissecting microscope (Carl Zeiss, Thornwood, NY). Videos were captured by using a standard CCD camera at 20 frames per sec.

SPIM. Videos of the cardiac conduction wave were recorded with SPIM (22). The attenuated 488-nm laser line from a DPSS laser (Sapphire 30 mW; Coherent, Santa Clara, CA) was focused to a 6-μm-thick light sheet. The sample was oriented such that a thin slice of atrium, AV canal, and ventricle was illuminated. The fluorescence was collected with a (20×/0.5) objective lens (Leica, Wetzlar, Germany) and an emission filter (HQ 525/50m; Chroma Technology Corp., Rockingham, VT) and imaged on an EM-CCD camera (DV885, 8-μm pixel size, binning 2; Andor, Belfast, Northern Ireland). Only a small area of the chip was read out, yielding a frame rate of ≈90 frames per sec. The microscope and camera were controlled with a Labview (National Instruments, Austin, TX) program, and images were saved in a binary format. After acquisition, the video sequences were analyzed with Matlab (The Mathworks, Natick, MA). In each sequence, several areas 15 × 15 pixels wide (i.e., 12 × 12 μm) were selected, and the intensity in these areas was plotted over time. All plots were semilogarithmic and identically scaled.

Morpholino Injections (*tnnt2* and *kcnh2*). We used a morpholino oligonucleotide targeted against the translational start site of *kcnh2* (National Center for Biotechnology Information sequence no. NM_212837) with the following sequence: 5′-CGCGTGGACA-GATTCAAGAGCCCTC-3′. The *silent heart* (*sih*/*tnnt2*) ATG morpholino was used as previously described (23).

AP Recordings from Embryonic Heart. Forty-eight hpf embryos were dechorionated and anesthetized with 0.02% tricaine for 1 to 2 min. The heart was dissected from the thorax *en bloc* by using fine forceps and transferred to the recording chamber. Only spontaneously beating whole hearts were studied. All experiments were performed at 22–24°C. The recording chamber was perfused with solution containing 140 mM NaCl, 4 mM KCl, 1.8 mM $CaCl_2$, 1 mM $MgCl_2$, 10 mM glucose, and 10 mM Hepes (pH 7.4). Suction pipettes were made from borosilicate capillary tubes (8,250 glass; A-M Systems, Sequim, WA) and fire-polished to obtain resistances of 6–9 MΩ when filled with 120 mM KCl, 5 mM EGTA, 5 mM K_2ATP, 10 mM Hepes, and 5 mM $MgCl_2$ (pH 7.2). Transmembrane potential (V_m) was measured by using an Axoclamp 2A amplifier (Molecular Devices, Sunnyvale, CA) in the bridge mode. V_m was measured with the disrupted patch technique. The pipette was positioned adjacent to the heart and a seal was formed by application of minimal suction. Using this technique, stable spontaneous APs were recordable for up to 2 h. Ventricular APs were generated by spontaneous electrical activity emanating from the atrium. V_m was filtered at 10 kHz and digitized at a sampling frequency of 20 kHz with a 12-bit analog-to-digital converter (Digidata 1322A Interface; Molecular Devices). AP duration from a series of five or more APs was calculated as the time interval between the peak maximum upstroke velocity (phase 0) and the time at 90% of repolarization (APD_{90}). To determine the effective refractory period, the heart was paced by injecting pulses of depolarizing current (1.5× threshold, 3 msec duration) at a cycle length of 350 msec for the atrium and 400 msec for the ventricle. Ten consecutive stimuli were followed by a single premature stimulus at progressively shorter coupling intervals.

Measurement of Electrocardiograms. Electrocardiograms were performed on adult zebrafish by using a protocol modified from

Milan *et al*. (11). The fish were anesthetized by immersion in 0.02% tricaine solution and placed ventral surface up in the recording chamber. Pancuronium (0.01 ml, 0.005 mg/ml) was injected into the peritoneal cavity to paralyze the gill musculature. The fish were orally perfused with a solution containing 5 mM NaCl, 0.17 mM KCl, 0.33 mM $CaCl_2$, 0.33 mM $MgSO_4$, and 10 mM Hepes (pH 7.5). Two stainless steel electrodes were inserted into the thorax on either side of the midline. A reference electrode was inserted more distally toward the tail. The bath electrode consisted of an Ag/AgCl pellet. The electrocardiogram signals were amplified by using a custom-built differential amplifier with a gain of 1,100 and a frequency bandwidth of 0.03–500 Hz. The signal was digitized by using a Digidata 1322A interface (Molecular Devices) and acquired at a rate of 1,000 Hz in gap-free mode by using Axoscope v9.2 (Molecular Devices). The QT interval was defined as the time from the upstroke of the QRS complex to the end of the T wave. Heart rate was measured as the time interval between the peaks of two consecutive QRS complexes (RR interval). To determine the relationship between QT interval and heart rate, the QT and RR intervals were plotted and fitted to the following equation by using a Levenberg–Marquardt least squares algorithm (Origin v7.5 graphing software; OriginLab, Northampton, MA): $QT = QTc*RR^{\alpha}$, as reported in ref. 11. The QT interval was corrected for heart rate by using the equation: $QTc = QT/RR^{\alpha}$.

We thank all members of the D.Y.R.S. Laboratory for support during the screen; A. Ayala, S. Waldron, and N. Zvenigorodsky for expert help with the fish; and J. R. Rigby and M. Arias for expert technical assistance. This work was supported by National Institutes of Health Grant K08 NHLBI (to N.C.C.), the Sarnoff Cardiovascular Research Foundation (R.A.), a Human Frontier Science Program Organization postdoctoral fellowship (to J.H.), National Institutes of Health grants (to K.S., M.T.-F., and D.Y.R.S.), the Nora Eccles Treadwell Foundation (K.S.), Fellow-to-Faculty American Heart Association awards (to N.C.C.), and the Packard Foundation (D.Y.R.S.).

1. Sehnert AJS, Stainier DYR (2002) *Trends Genet* 18:419–424.
2. Splawski I, Shen J, Timothy KW, Lehmann MH, Priori S, Robinson JL, Moss AJ, Schwartz PJ, Towbin JA, Vincent GM, *et al.* (2000) *Circulation* 102:1178–1185.
3. Hoorntje T, Alders M, van Tintelen P, van der Lip K, Sreeram N, van der Wal A, Mannens M, Wilde A (1999) *Circulation* 100:1264–1267.
4. Schwartz PJ, Stramba-Badiale M (2004) *Prolonged Repolarization and Sudden Infant Death Syndrome* (Saunders, Philadelphia).
5. Babij P, Askew GR, Nieuwenhuijsen B, Su CM, Bridal TR, Jow B, Argentieri TM, Kulik J, DeGennaro LJ, Spinelli W, *et al.* (1998) *Circ Res* 83:668–678.
6. Nerbonne JM (2004) *Trends Cardiovasc Med* 14:83–93.
7. Salama G, London B (2007) *J Physiol* 578:43–53.
8. Lee MP, Ravenel JD, Hu RJ, Lustig LR, Tomaselli G, Berger RD, Brandenburg SA, Litzi TJ, Bunton TE, Limb C, *et al.* (2000) *J Clin Invest* 106:1447–1455.
9. Sedmera D, Reckova M, deAlmeida A, Sedmerova M, Biermann M, Volejnik J, Sarre A, Raddatz E, McCarthy RA, Gourdie RG, *et al.* (2003) *Am J Physiol Heart Circ Physiol* 284:H1152–H1160.
10. Kopp R, Schwerte T, Pelster B (2005) *J Exp Biol* 208:2123–2134.
11. Milan DJ, Jones IL, Ellinor PT, MacRae CA (2006) *Am J Physiol Heart Circ Physiol* 291:H269–H273.
12. Chen JN, Haffter P, Odenthal J, Vogelsang E, Brand M, van Eeden FJ, Furutani-Seiki M, Granato M, Hammerschmidt M, Heisenberg CP, *et al.* (1996) *Development (Cambridge, UK)* 123:293–302.
13. Stainier DY, Fouquet B, Chen JN, Warren KS, Weinstein BM, Meiler SE, Mohideen MA, Neuhauss SC, Solnica-Krezel L, Schier AF, *et al.* (1996) *Development (Cambridge, UK)* 123:285–292.
14. Stainier DY (2001) *Nat Rev Gen* 2:39–48.
15. Beis D, Bartman T, Jin SW, Scott IC, D'Amico LA, Ober EA, Verkade H, Frantsve J, Field HA, Wehman A, *et al.* (2005) *Development (Cambridge, MA)* 132:4193–4204.
16. Langheinrich U, Vacun G, Wagner T (2003) *Toxicol Appl Pharmacol* 193:370–382.
17. Sanguinetti MC, Curran ME, Spector PS, Keating MT (1996) *Proc Natl Acad Sci USA* 93:2208–2212.
18. Taggart P, Sutton PM, Boyett MR, Lab M, Swanton H (1996) *Circulation* 94:2526–2534.
19. Maltsev VA, Wobus AM, Rohwedel J, Bader M, Hescheler J (1994) *Circ Res* 75:233–244.
20. Salata JJ, Jurkiewicz NK, Wallace AA, Stupienski RF III, Guinosso PJ, Jr, Lynch JJ, Jr (1995) *Circ Res* 6:110–119.
21. Nakai J, Okhura M, Imoto K (2001) *Nat Biotechnol* 19:137–141.
22. Huisken J, Swoger J, Del Bene F, Wittbrodt J, Stelzer EH (2004) *Science* 305:1007–1009.
23. Sehnert AJ, Huq A, Weinstein BM, Walker C, Fishman M, Stainier DY (2002) *Nat Genet* 31:106–110.
24. Roy M-L, Dumaine R, Brown AM (1996) *Circ Res* 94:817–823.
25. Milan DJ, Giokas AC, Serluca FC, Peterson RT, MacRae CA (2006) *Development (Cambridge, UK)* 133:1125–1132.
26. Fraser GR, Froggatt P, Murphy T (1964) *Ann Hum Genet* 28:133–157.
27. Huang CJ, Tu CT, Hsiao CD, Hsieh FJ, Tsai HJ (2003) *Dev Dyn* 228:30–40.